Electrochromic Iridium Oxide Films: Compatibility with Propionic Acid, Potassium Hydroxide, and Lithium Perchlorate in Propylene Carbonate

R.-T. Wen*, G. A. Niklasson and C. G. Granqvist

Department of Engineering Sciences, The Ångström Laboratory, Uppsala University, P. O. Box 534, SE-75121 Uppsala, Sweden

Abstract

Porous thin films of Ir oxide were prepared by reactive dc magnetron sputtering onto unheated substrates. The crystallite size was ~5 nm, and a small amount of unoxidized Ir was present. The electrochromic performance was studied by optical transmittance measurements and cyclic voltammetry applied to films in aqueous and non-aqueous electrolytes, specifically being 1M propionic acid, 1M potassium hydroxide (KOH), and 1M lithium perchlorate in propylene carbonate (Li–PC). Cyclic voltammetry measurements indicated that the films had a fractal surface structure. Good electrochromism, with mid-luminous transmittance modulation between ~55 and ~90 % in ~100-nm-thick films, was documented in all of the electrolytes.

Keywords: Ir oxide, porous thin films, electrochromism, transmittance, durability

*Corresponding author: Ruitao.Wen@angstrom.uu.se

1. Introduction

Electrochromic (EC) thin films show reversible and persistent changes of their optical properties under charge insertion/extraction [1–3] and have many applications in contemporary technology such as for energy saving and comfort-enhancing "smart" windows and glass facades in buildings [4–7], high-performance information displays, "anti-dazzling" rear-view mirrors for cars, variable-emittance surfaces for thermal control, etc. The most widely studied EC device incorporates five superimposed layers: an electrolyte is in the middle and connects an EC film to an ion-storage film (ideally also with EC properties), and this three-layer configuration is embedded between transparent and electrically conducting films. Optical changes are effected when a voltage is applied between the transparent conductors and are related to joint insertion of electrons from the transparent electrodes and ions from the electrolyte into the EC film(s).

There are two types of EC thin films: one is called "cathodic" and colors under ion insertion and the other is called "anodic" and colors under ion extraction. Oxides based on W, Mo, Nb, and Ti are examples of the first type, and oxides of Ir, Ni, and Co belong to the second type. Combinations of one cathodic and another anodic EC film are favorable from an optical point of view, and devices incorporating W oxide, Ni oxide, and an intervening polymer electrolyte have been studied in particular detail during the last decade [8,9].

The purpose of this paper is to lay the foundation for in-depth studies of Ir-oxide-based films, which are interesting from a fundamental perspective and also for special applications requiring EC devices with particularly good optical performance and/or durability. Ir oxide has been studied in this context at least since 1978 [10,11], and sputter deposited EC films were reported in 1979 [12]; the early literature has been reviewed in detail [1]. The research field maintains its vitality [13–20]. Concerning durability, we notice that Ir oxide films have undergone EC cycling for up to 7×10^6 ion insertion/extraction cycles without significant degradation [21]. Ir is a rare element in the earth's crust and available only at a few geographical locations, which gives obvious restrictions for applications. However, it should be noticed that significant electrochromism prevails in Ir oxide even after dilution with less costly Ta [16,19] and Sn [17,18,20].

Specifically, we report below on the compatibility of porous Ir oxide films with three electrolytes: 1M propionic acid (CH_3CH_2COOH; aqueous and acidic), 1M KOH (potassium

hydroxide; aqueous and basic), and 1M lithium perchlorate in propylene carbonate ($LiClO_4$ in $C_4H_6O_3$, denoted Li–PC; non-aqueous). The electrochemical reactions underlying the electrochromism in these types of electrolytes have been the subject of much interest over the years [1]. Thus, for aqueous electrolytes, a cation (proton) process is expected to progress according to

$$IrO_x(OH)_{3-x} + xH^+ + xe^- \leftrightarrow Ir(OH)_3 , \quad (1)$$

whereas an anion (hydroxyl) process can be described as

$$Ir(OH)_{3+x} - xOH^- + xe^- \leftrightarrow Ir(OH)_3 , \quad (2)$$

where e^- denotes electrons and x can be as large as unity. Reaction (2) is highly schematic, and the reason for the electrochromism may in fact be the splitting of water molecules and ensuing insertion and extraction of protons. $Ir(OH)_3$ represents the transparent state; it can be written alternatively as $HIrO_2 \cdot H_2O$ or $IrOOH \cdot H_2O$. At $x = 1$, the colored oxide can be written as $IrO_2 \cdot H_2O$ for the cation process and $IrO_2 \cdot 2H_2O$ for the anion process. With regard to the Li-containing electrolyte, the corresponding reaction is

$$IrO_2 + xLi^+ + xe^- \leftrightarrow Li_xIrO_2 . \quad (3)$$

Our present study can be viewed as a counterpart to our earlier investigation on the compatibility of Ni oxide with different electrolytes [22].

2. Experimental

2.1 Thin film deposition

Thin films of Ir oxide were prepared by reactive dc magnetron sputtering in a deposition system based on a Balzers UTT 400 unit. The substrates were unheated 5 × 5 cm^2 glass plates pre-coated with transparent and electrically conducting layers of In_2O_3:Sn (known as ITO) with a sheet resistance of 60 Ω. Some films were deposited also onto carbon plates. The target was a 5-cm-diameter cylindrical plate of metallic Ir (99.95 %). Pre-sputtering took place in argon (99.998 %) for 3 minutes, and oxygen (99.998 %) was then introduced so that the O_2/Ar gas-flow ratio remained at a constant value within the $0.5 \leq \gamma \leq 2$ range. The target–substrate separation was 13 cm. The total pressure during sputtering was set to 30 mTorr, and the power at the target was 200 W.

The film thickness was determined by surface profilometry using a DektakXT instrument and lay in the $30 \leq d \leq 700$ nm range.

2.2 Structural and compositional characterization

Film structures were determined by X-ray diffraction (XRD) using a Siemens D5000 instrument operating with CuK_α radiation at a wavelength λ_x = 0.154 nm. Specific assignments and inferences about preferred orientations were obtained by comparison with the Joint Committee on Powder Diffraction Standards (JCDPS) data base.

The grain size D was determined from Scherrer's formula [23], i.e.,

$$D = \frac{k\lambda_x}{\beta \cos\theta} \quad , \tag{4}$$

where $k \sim 0.9$ is a dimensionless "shape factor", β is the full width at half-maximum of an X-ray diffraction peak, and θ is the diffraction angle.

The morphology of the Ir oxide films was characterized by scanning electron microscopy (SEM) using a LEO 1550 FEG Gemini instrument with an acceleration voltage of 10 to 15 kV.

Elemental compositions and atomic concentrations were determined by Rutherford Backscattering Spectroscopy (RBS) at the Uppsala Tandem Laboratory, specifically using 2MeV ^{4}He ions back scattered at an angle of 172 degrees. The RBS data were fitted to a model of the film–substrate system by use of the SIMNRA program [24].

The film density ρ was computed from

$$\rho = \frac{M \cdot N_s}{n_{atoms} \cdot N_A d} \quad , \tag{5}$$

where M is molar mass, N_s is thickness in atoms/cm^2, n_{atoms} is number of atoms in a molecule, N_A is Avogadro's constant, and d is thickness in centimeters.

2.3 Electrochemical and optical measurements

Cyclic voltammetry (CV) was performed in a three-electrode electrochemical cell by use of a computer-controlled ECO Chemie Autolab/GPES Interface. The Ir oxide film served as working electrode and was electrochemically cycled in three electrolytes: 1M propionic acid, 1M KOH, and 1M Li–PC. For propionic acid and KOH, the counter electrode was a Pt foil

and the reference electrode was Ag/AgCl; the voltage ranges were chosen as –0.5 to 1.25 V vs Ag/AgCl for propionic acid and –1.2 to 0.5 V vs Ag/AgCl for KOH, in order to get the same anodic and cathodic charge density while avoiding electrolyte decomposition. The pH value is 2.2 and 14 for propionic acid and KOH, respectively. In the case of Li–PC, both counter and reference electrodes were Li foils, and the voltage range was 2.0 to 4.7 V vs Li. The low voltage limit was chosen to avoid irreversible formation of Li_2O and LiOH [25] as well as electro-activity in ITO [25,26]; the high voltage limit was set to avoid oxidation of PC [27,28]. The voltage sweep rate lay in the $2 < \nu < 50$ mV/s range.

Optical transmittance measurements were recorded *in situ* during electrochemical cycling of Ir oxide films at the fixed wavelength $\lambda = 550$ nm by use of a fiber-optical instrument from Ocean Optics. The electrochemical cell was positioned between a tungsten halogen lamp and the detector, and the 100-%-level was taken as the transmittance recorded before immersion of the sample in the electrolyte.

Electrochemical and optical measurements were combined to determine the coloration efficiency (CE), defined as the difference in optical density per amount of charge exchange (ΔQ). Data were obtained from

$$CE = \frac{\ln\left(\frac{T_{bleached}}{T_{colored}}\right)}{\Delta Q} \quad , \qquad (6)$$

where $T_{bleached}$ and $T_{colored}$ are the transmittance values for the bleached and colored states, respectively, and it is presumed that the associated reflectance modulation is insignificant. For most EC devices—including "smart" windows—it is desirable to have a large CE.

3. Results and discussion

3.1 Structure and composition

Fig. 1 shows XRD data for Ir oxide films deposited with the shown values of the O_2/Ar gas flow ratio onto glass and ITO-coated glass. The uppermost curve refers to a 700-nm-thick film deposited at $\gamma = 1.0$ and indicates one distinct diffraction peak at $2\theta = 34.7°$ together with weaker diffraction peaks at $2\theta = 28.1°$ and $2\theta = 40.1°$. The former two of these features can be assigned to the (110) and (101) reflections in the rutile phase of IrO_2 (JCPDS Card 18–870), respectively, whereas the third feature is assigned to (111) reflections of metallic Ir in

the fcc phase (JCPDS Card 46–1044). The high relative intensity of the (101) reflection in IrO_2 indicates preferential crystalline orientation. The large width of this diffraction feature signifies a small grain size, and Eq. 4 yielded that $D \approx 5$ nm. The grain size found for the present samples is consistent with the value 3 to 4 nm reported from XRD line broadening as well as transmission electron microscopy in earlier work [15,29].

The bottom curve in Fig. 1 was taken on an ITO film on glass and shows a series of diffraction peaks ascribed to the indicated reflections (JCPDS Card 06–0416). The remaining four diffractograms in Fig. 1, for Ir oxide films with $65 \leq d \leq 180$ nm and deposited onto ITO-coated glass, show traces of the (101) reflections in IrO_2 (except in the thinnest Ir oxide film), whereas all of the other diffraction features originate from ITO. The Ir oxide films were sputter deposited with four different gas flow ratios in the $0.5 \leq \gamma \leq 2$ range. No significant differences in the diffractograms can be associated with the relative oxygen content.

It is apparent from Fig. 1 that some small fraction of unoxidized Ir can remain in the sputter deposited films, which is not unexpected considering its inertness. Results similar to ours have been reported in other work on Ir oxide films made by reactive sputter deposition [30–33], reactive pulsed laser deposition [34] and atomic layer deposition [35], especially if the oxygen content was limited.

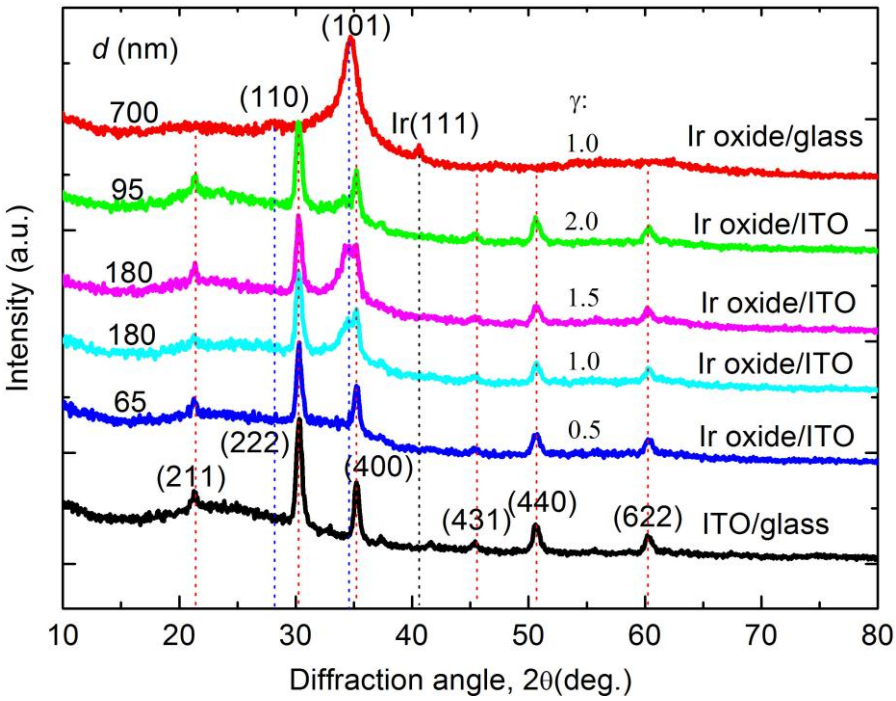

Fig. 1. X-ray diffractograms taken for films of Ir oxide and ITO, and for four Ir oxide films on ITO. Thickness d and O_2/Ar ratio γ during sputtering are given for the Ir oxide films. All films were backed by glass. The diffraction peaks are assigned to the shown reflections, and their locations are indicated by vertical dotted lines.

RBS was used to record the elemental compositions of the Ir oxide films as a function of O_2/Ar gas flow ratio during sputter deposition. Fig. 2 shows that the value of z in IrO_z went from ~2.1 to ~2.8 for films deposited at successively larger values of γ, from 0.5 to 2. At γ = 1.0 we found $z \approx 2.6$, which is slightly larger than the value 2.4 reported in earlier work [15].

The densities of the films were assessed by use of Eq. 5. It was found that ρ decreased from 6.4 to 3.9 g/cm^3 as γ was increased from 0.5 to 2. All of these values are much lower than 11.6 g/cm^3, which pertains to bulk crystalline IrO_2, meaning that our Ir oxide films exhibit large porosity. The substantial oxygen excess at the largest porosity is tentatively ascribed to water molecules and/or OH groups on internal surfaces in the Ir oxide films.

Fig. 3 shows a SEM image of an Ir oxide film deposited at γ = 1.0. The grains are filamentary-like and interconnected to form a very porous structure. Other Ir oxide films, deposited with different values of γ, had a similar morphology.

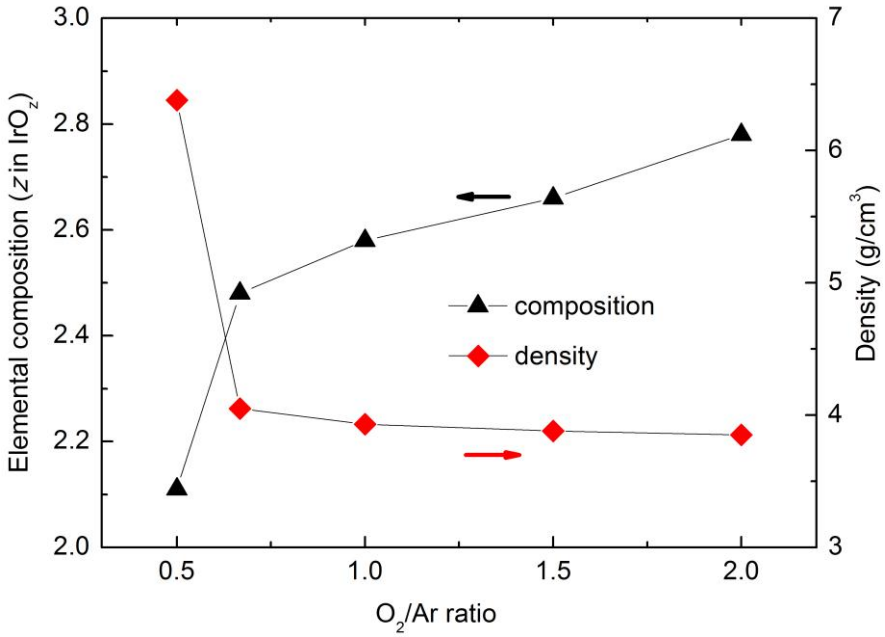

Fig. 2. Elemental composition, given as z in IrO_z, and density for Ir oxide films sputter deposited at the shown O_2/Ar ratios. Data points are connected by lines for convenience. Arrows indicate the pertinent vertical scale.

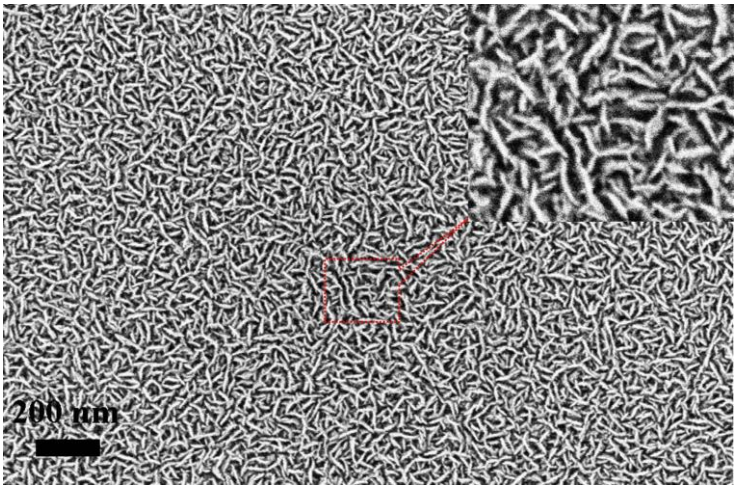

Fig. 3. SEM image of an Ir oxide film sputter deposited at an O_2/Ar ratio of 1.0. The insert shows a magnification of the indicated area.

3.2 Electrochemical properties

Cyclic voltammetry was applied to Ir oxide films prepared with the O_2/Ar ratios 0.5, 1 and 2 and having similar thicknesses, specifically being ~70, 100 and 95 nm, respectively. Data are shown in Figs. 4(a)–(c) for films immersed in propionic acid, KOH and Li–PC, respectively, and refer to the second CV cycle. The voltage sweep rate was 10 mV/s. The data are in overall agreement with earlier ones [1,14]. The main conclusion is that our various films displayed consistent CVs—meaning that the precise magnitude of the O_2/Ar ratio was not critical—and that the data were qualitatively different for recordings made in aqueous (Figs. 4a and b) and non-aqueous (Fig. 4c) electrolytes. This is expected considering the different electrochemical reactions in Eqs. (1)-(3), but a detailed explanation of the features of the CV's is not yet available.

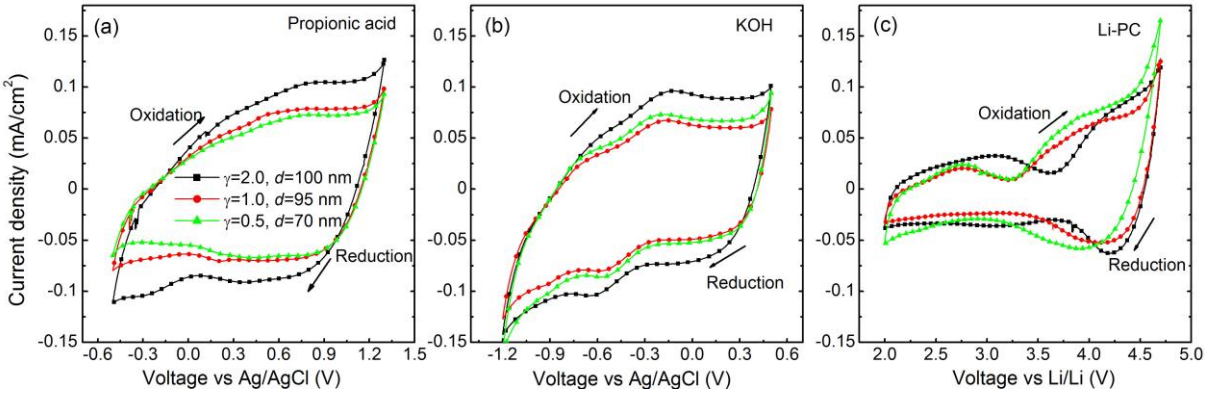

Fig. 4. Cyclic voltammograms showing current density vs voltage for Ir oxide films sputter deposited at the shown O_2/Ar ratios γ to the stated thicknesses *d*. Data were taken at the second CV cycle and

were recorded at 10 mV/s. Panels (a), (b) and (c) refer to measurements in propionic acid, KOH and Li–PC, respectively. Arrows signify voltage sweep direction.

Fig. 5 reports CV data on the effect of varying voltage sweep rates for a film characterized by γ = 1.0 and d = 180 nm and immersed in propionic acid. The symmetrical nature of the voltammograms signals that the inserted and extracted charge densities are equal, i.e., that electrochemical reversibility prevails.

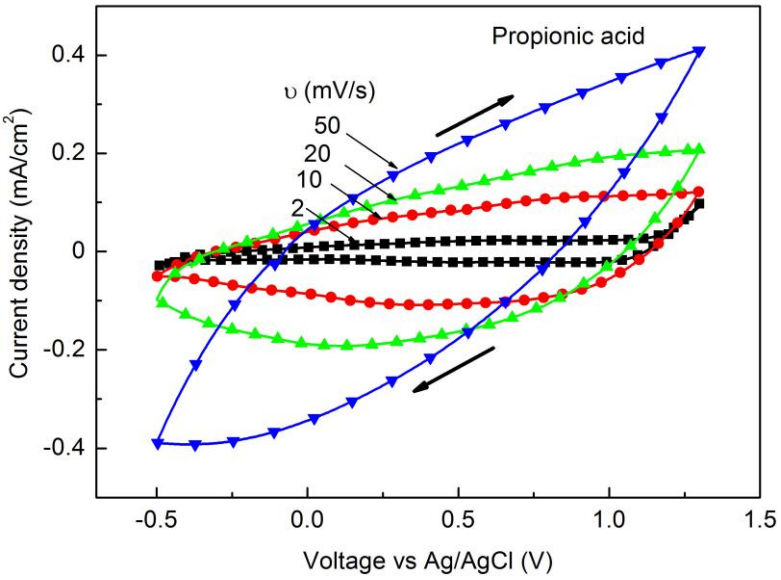

Fig. 5. Cyclic voltammograms showing current density vs voltage for Ir oxide films sputter deposited at the O_2/Ar ratio γ=1.0 to the thickness d=180 nm and immersed in propionic acid. Data were taken at the second CV cycle and were recorded at four values of the voltage sweep rate ν. Arrows signify voltage sweep direction.

The inserted and extracted charge densities depend on the voltage sweep rate, as illustrated in Fig. 6(a), and decrease monotonically as v is increased from 2 to 50 mV/s. Fig. 6(b) displays peak current density measured in both the cathodic and anodic sweep direction for the CVs in Fig. 5. The data are found to obey a linear relationship with a slope of 0.91 when plotted on a log–log diagram, which is consistent with ion diffusion towards an electrode characterized by a fractal surface, as discussed before for Ir-oxide-based films [14]. Specifically, a modified Randles–Sevčik equation [36] yields that the fractal dimension is 2.82.

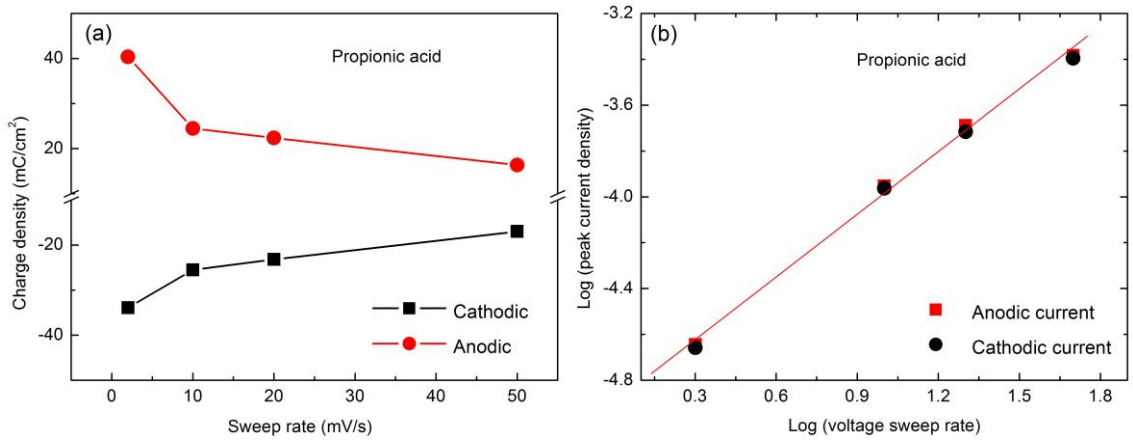

Fig. 6. Panel (a) shows maximum charge density during ion insertion and extraction at different voltage sweep rates as extracted from Fig. 5. Data points are connected by straight lines for convenience. Panel (b) reports log(peak current density) vs log(voltage sweep rate). The peak current density, in units of mA/cm^2, was extracted from Fig. 5 and the voltage sweep rate is in units of mV/s. The straight line was drawn as a fit to these data.

3.3 Electrochromism

Fig. 7 reports on a comprehensive set of measurements on Ir oxide films deposited with γ = 1.0, having the thicknesses 30, 65 and 100 nm, and immersed in propionic acid, KOH and Li–PC. Figures 7(a)–(c) display CVs recorded at ν = 10 mV/s that are consistent with the data in Fig. 5 and indicating, expectedly, that the charge density increases in proportion with the thickness. Figures 7(a')–(c') show corresponding optical modulation for 50 minutes during CV cycles and shows that the transmittance is varied for ~100-nm-thick films between a lower level of ~55 % and an upper level of ~90 % for each of the electrolytes. The bleached-state transmittance was somewhat lower for measurements in KOH than in the other electrolytes. A slight drift of the transmittance can be noted for the film immersed in KOH, irrespectively of the magnitude of γ; the reason for this effect is unclear so far. Thin films naturally do not attain as small transmittance as thick films, and films with *d* being 30 and 65 nm show a minimum transmittance level of ~65 % and ~75 %, respectively, while the maximum transmittance level is relatively insensitive to film thickness. Table I reports values of maximum charge density for ion insertion and extraction, as well as corresponding coloration efficiency calculated from Eq. 6. The CEs are 18.5 ± 2.0, 14.0 ± 2.5, and 23.5 ± 3.0 cm^2/C for films immersed in propionic acid, KOH and Li–PC, respectively. These values are of the expected order of magnitude [1], though somewhat on the high side for Li–PC.

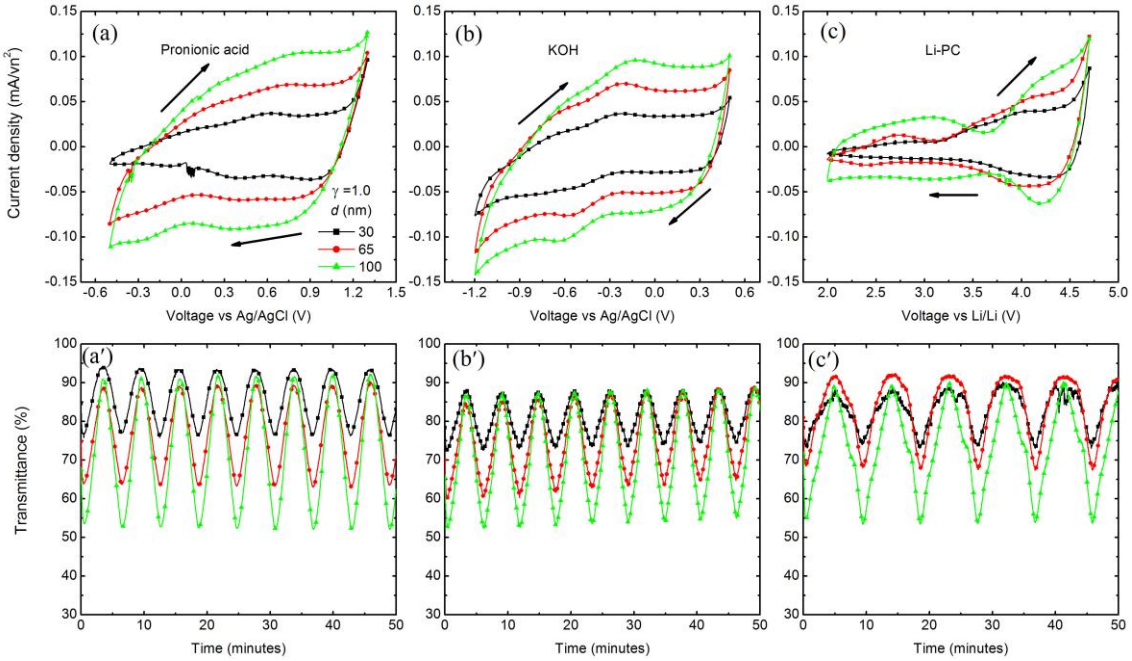

Fig. 7. Upper panels report cyclic voltammograms showing current density vs voltage for Ir oxide films sputter deposited at the shown O_2/Ar ratio γ to the stated thicknesses *d* and immersed in three electrolytes. Data were taken at the second CV cycle and were recorded at a voltage sweep rate of 10 mV/s. Arrows signify voltage sweep direction. Lower panels report corresponding optical transmittance modulation at a wavelength of 550 nm.

Table 1. Maximum charge density and coloration efficiency for Ir oxide films immersed in different electrolytes. The data are based on the measurements reported in Fig. 7.

Thickness	Charge density (mC/cm^2)			Coloration efficiency (cm^2/C)		
(nm)	Propionic acid	KOH	Li–PC	Propionic acid	KOH	Li–PC
30	9.2	15.1	8.3	20.5	11.5	20.8
65	20.5	23.5	13.5	16.5	13.3	22.4
100	29.2	30.7	19.5	18.7	16.3	26.6

3.4 Durability assessment

Durability for up to 2000 voltammetric cycles was performed at ν = 50 mV/s for ~100-nm-thick Ir oxide films deposited at γ = 1.0. Fig. 8 reports data for three electrolytes and shows that some minor changes have evolved after 1000 cycles, whereas there are almost no further changes during 1000 additional cycles. Hence stable electrochemical properties exist in all the electrolytes, which is the expected result [1]. This stability was documented also

through charge density and transmittance measurements, which are consistent with the CV data.

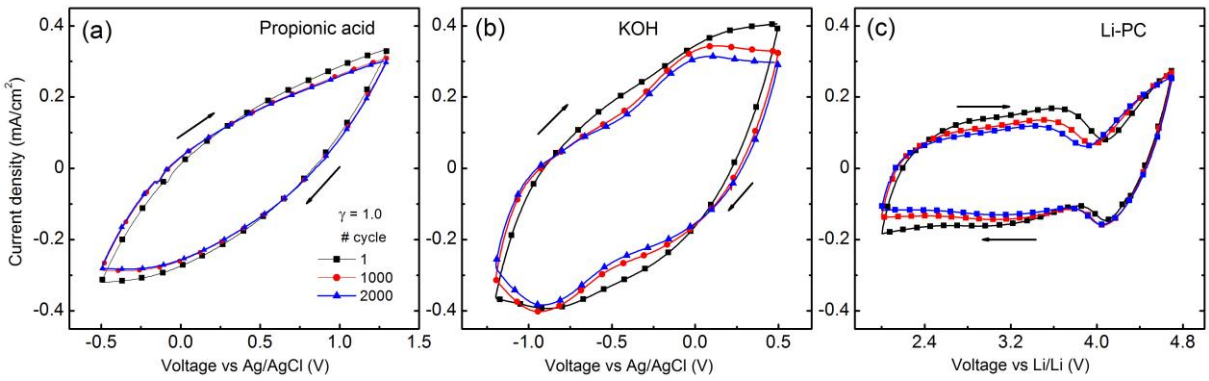

Fig. 8. Cyclic voltammograms showing current density vs voltage for Ir oxide films sputter deposited at the shown O_2/Ar ratio γ to the stated thickness *d* and immersed in three electrolytes. Data were taken at the indicated numbers of CV cycles and were recorded at a voltage sweep rate of 50 mV/s. Arrows signify voltage sweep direction.

4. Summary and conclusion

Thin films of Ir oxide were prepared by reactive dc magnetron sputtering onto unheated substrates. XRD showed that the crystallite size was ~5 nm and that a small amount of unoxidized Ir was present. RBS and thickness measurements yielded that the film porosity was large. SEM characterization indicated that the films were highly porous and dominated by a filamentary-like structure. The EC performance was investigated by optical transmittance measurements and cyclic voltammetry applied to films in aqueous and non-aqueous electrolytes, specifically being 1M propionic acid, 1M potassium hydroxide (KOH), and 1M lithium perchlorate in propylene carbonate (Li–PC). Peak currents in cyclic voltammetry measurements performed at different scan rates were analyzed and it was found that the surface of Ir oxide exhibited a fractal structure. Good electrochromism, with mid-luminous transmittance modulation between ~55 and ~90 % in ~100-nm-thick films, was documented in all of the electrolytes. Our results serve as a basis for further in-depth studies of Ir-oxide-based electrochromic films and devices based on those.

Acknowledgement: We acknowledge support with RBS-measurements from Daniel Primetzhofer and the staff of the Tandem accelerator laboratory at Uppsala University. This work was financially supported by the European Research Council under the European Community's Seventh Framework Program (FP7/2007–2013)/ERC Grant Agreement No.

267234(GRINDOOR).

References

[1] C.G. Granqvist, Handbook of Inorganic Electrochromic Materials, Elsevier, Amsterdam, The Netherlands, 1995.

[2] C.G. Granqvist, Electrochromic tungsten oxide films: Review of progress 1993–1998, Solar Energy Materials and Solar Cells 60 (2000) 201–262.

[3] P.M.S. Monk, R.J. Mortimer, D.R. Rosseinsky, Electrochromism and Electrocromic Devices, Cambridge University Press, Cambridge, UK, 2007.

[4] R. Baetens, B.P. Jelle, A. Gustavsen, Properties, requirements and possibilities of smart windows for dynamic daylight and solar energy control in buildings: A state-of-the-art review, Solar Energy Materials and Solar Cells 94 (2010) 87–105.

[5] G.B. Smith, C.G. Granqvist, Green Nanotechnology: Solutions for Sustainability and Energy in the Built Environment, CRC Press, Boca Raton, FL, USA, 2010.

[6] C.G. Granqvist, Oxide electrochromics: An introduction to devices and materials, Solar Energy Materials and Solar Cells 99 (2012) 1–13.

[7] B.P. Jelle, A. Hynd, A. Gustavsen, D. Arasteh, H. Goudey, R. Hart, Fenestration of today and tomorrow: A state-of-the-art review and future research opportunities, Solar Energy Materials and Solar Cells 96 (2012) 1–28.

[8] A. Azens, G. Gustavsson, R. Karmhag, C.G. Granqvist, Electrochromic devices on polyester foil, Solid State Ionics 165 (2003) 1–5.

[9] G.A. Niklasson, C.G. Granqvist, Electrocromics for smart windows: Thin films of tungsten oxide and nickel oxide, and devices based on these, Journal of Materials Chemistry 17 (2007) 127–156.

[10] G. Beni, J.L. Shay, Electrochromism of heat-treated anodic iridium oxide films in acidic, neutral, and alkaline solutions, Applied Physics Letters 33 (1978) 567–568.

[11] S. Gottesfeld, J.D.E. McIntyre, G. Beni, J.L. Shay, Electrochromism in anodic iridium oxide films, Applied Physics Letters 33 (1978) 208–210.

[12] L.M. Schiavone, W.C. Dautremont-Smith, G. Beni, J.L. Shay, Electrochromic iridium oxide films prepared by reactive sputtering, Applied Physics Letters 35 (1979) 823–825.

[13] A. Azens, C.G. Granqvist, Electrochromism of Ir–Mg oxide films, Applied Physics Letters 81 (2002) 928–930.

[14] J. Backholm, A. Azens, G.A. Niklasson, Electrochemical and optical properties of sputter deposited Ir–Ta and Ir oxide thin films, Solar Energy Materials and Solar Cells 90 (2006) 414–421.

[15] J. Backholm, E. Avendano, A. Azens, G. de M. Azevedo, E. Colonel, G.A. Niklasson, C.G. Granqvist, Iridium-based oxides : Recent advances in coloration mechanism, structural and morphological characterization, Solar Energy Materials and Solar Cells 92 (2008) 91–96.

[16] J. Backholm, G.A. Niklasson, Optical properties of electrochromic iridium oxide and iridium–tantalum oxide thin films in different colouration states, Solar Energy Materials and Solar Cells 92 (2008) 1388–1392.

[17] T. Niwa, O. Takai, All-solid-state reflectance-type electrochromic devices using iridium tin oxide film as counter electrode, Thin Solid Films 518 (2010a) 5340–5344.

[18] T. Niwa, O. Takai, Electrochemical, optical and electronic properties of iridium tin oxide thin film as counter electrode of electrochromic device, Japanese Journal of Applied Physics 49 (2010b) 105802/1–105802/5.

[19] S.U. Yun, S.J. Yoo, J.W. Lim, S.H. Park, I.Y. Cha, Y.-E. Sun, Enhanced electrochromic properties of Ir–Ta oxide grown using a cosputtering system, Journal of the Electrochemical Society 157 (2010) J256–J260.

[20] S. Harada, K. Yoshino, S. Fukudome, Y. Kawano, F. Sei, Growth of IrO_x–SnO_x films deposited by reactive sputtering, Japanese Journal of Applied Physics 50 (2011) 05FB14/1–05FB14/2.

[21] K. Yamanaka, Anodically electrodeposited iridium oxide films (AEIROF) from alkaline solutions for electrochromic display devices, Japanese Journal of Applied Physics 28 (1989) 632–637.

[22] S. Green, J. Backholm, P. Georen, C.G. Granqvist, G.A. Niklasson, Electrochromism in nickel oxide and tungsten oxide thin films: Ion intercalation from different electrolytes, Solar Energy Materials and Solar Cells 93 (2009) 2050–2055

[23] B.D. Cullity, S.R. Stock, Elements of X-ray Diffraction, 3rd ed., Prentice-Hall, Upper Saddle River, NJ, USA, 2001; pp. 167–171.

[24] M. Mayer, SIMNRA, a simulation program for the analysis of NRA, RBS and ERDA, American Institute of Physics Conference Proceedings 475 (1999) 541–544.

[25] P.M.M.C. Bressers, E.A Meulenkamp, The electrochromic behavior of indium tin oxide in propylene carbonate solutions, Journal of the Electrochemical Society 145 (1998) 2225–2230.

[26] A. Corradini, A.M. Marinangeli, M. Mastragostino, ITO as a counter-electrode in a polymer based electrochromic device, Electrochimica Acta 35 (1990) 1757–1760.

[27] D. Aurbach, M. Daroux, P. Faguy, E. Yeager, The electrochemistry of noble metal electrodes in aprotic organic solvents containing lithium salts, Journal of Electroanalytical Chemistry 297 (1991) 225–244.

[28] D. Pletcher, J.F. Rohan, A.G. Rithie, Microelectrode studies of the lithium/propylene carbonate system – Part I. Electrode reactions at potentials positive to lithium deposition, Electrochimica Acta 39 (1994) 1369–1376.

[29] K. Kreider, Summary abstract: IrO_2 radio frequency sputtered thin film properties, Journal of Vacuum Science and Technology A 4 (1986) 606–607.

[30] C.U. Pinnow, I. Kasko, C. Dehm, B. Jobst, M. Seibt, U. Geyer, Preparation and properties of dc-sputtered IrO_2 and Ir thin films for oxygen barrier applications in advanced memory technology, Journal of Vacuum Science and Technology B 19 (2001) 1857–1865.

[31] T. Ishikawa, Y. Abe, M. Kawamura, K. Sasaki, Formation process and electrical property of IrO_2 thin films prepared by reactive sputtering, Japanese Journal of Applied Physics 42 (2003) 213–216.

[32] S. Thanawala, D.G. Georgiev, R.J. Baird, G. Auner, Characterization of iridium oxide thin films deposited by pulsed-direct-current reactive sputtering, Thin Solid Films 515 (2007) 7059–7065.

[33] S. Negi, R. Bhandari, L. Rieth, F. Solzbacher, Effect of sputtering pressure on pulsed-DC sputtered iridium oxide films, Sensors and Actuators B 137 (2009) 370–378.

[34] M.A. El Khakani, M. Chaker, Reactive pulsed laser deposition of iridium oxide thin films, Thin Solid Films 335 (1998) 6–12.

[35] S.-W. Kim, S.-H. Kwon, D.-K. Kwak, S.-W. Kang, Phase control of iridium and iridium oxide thin films in atomic layer deposition, Journal of Applied Physics 103 (2008) 023517/1–023517/6.

[36] M. Strømme, G.A. Niklasson, C.G. Granqvist, Voltammetry on fractals, Solid State Communications 96 (1995) 151–154.

Table and Figure captions

Table 1. Maximum charge density and coloration efficiency for Ir oxide films immersed in different electrolytes. The data are based on the measurements reported in Fig. 7.

Fig. 1. X-ray diffractograms taken for films of Ir oxide and ITO, and for four Ir oxide films on ITO. Thickness *d* and O_2/Ar ratio γ during sputtering are given for the Ir oxide films. All films were backed by glass. The diffraction peaks are assigned to the shown reflections, and their locations are indicated by vertical dotted lines.

Fig. 2. Elemental composition, given as *z* in IrO_z, and density for Ir oxide films sputter deposited at the shown O_2/Ar ratios. Data points are connected by lines for convenience. Arrows indicate the pertinent vertical scale.

Fig. 3. SEM image of an Ir oxide film sputter deposited at an O_2/Ar ratio of 1.0. The insert shows a magnification of the indicated area.

Fig. 4.Cyclic voltammograms showing current density vs voltage for Ir oxide films sputter deposited at the shown O_2/Ar ratios γ to the stated thicknesses *d*. Data were taken at the second CV cycle and were recorded at 10 mV/s. Panels (a), (b) and (c) refer to measurements in propionic acid, KOH and Li–PC, respectively. Arrows signify voltage sweep direction.

Fig. 5. Cyclic voltammograms showing current density vs voltage for Ir oxide films sputter deposited at the O_2/Ar ratio γ=1.0 to the thickness *d*=180 nm and immersed in propionic acid. Data were taken at the second CV cycle and were recorded at four values of the voltage sweep rate ν. Arrows signify voltage sweep direction.

Fig. 6. Panel (a) shows maximum charge density during ion insertion and extraction at different voltage sweep rates as extracted from Fig. 5. Data points are connected by straight lines for convenience. Panel (b) reports log(peak current density) vs log(voltage sweep rate). The peak current density, in units of mA/cm^2, was extracted from Fig. 5 and the voltage sweep rate is in units of mV/s. The straight line was drawn as a fit to these data.

Fig. 7. Upper panels report cyclic voltammograms showing current density vs voltage for Ir oxide films sputter deposited at the shown O_2/Ar ratio γ to the stated thicknesses *d* and immersed in three electrolytes. Data were taken at the second CV cycle and were recorded at a voltage sweep rate of 10 mV/s. Arrows signify voltage sweep direction. Lower panels report corresponding optical transmittance modulation at a wavelength of 550 nm.

Fig. 8. Cyclic voltammograms showing current density vs voltage for Ir oxide films sputter deposited at the shown O_2/Ar ratio γ to the stated thickness *d* and immersed in three electrolytes. Data were taken at the indicated numbers of CV cycles and were recorded at a voltage sweep rate of 50 mV/s. Arrows signify voltage sweep direction.